Firing activities in a fractional-order Hindmarsh–Rose neuron with multistable memristor as autapse

Zhi-Jun Li(李志军)[1,†], Wen-Qiang Xie(谢文强)[1], Jin-Fang Zeng(曾金芳)[2], and Yi-Cheng Zeng(曾以成)[2]

[1] *School of Automation and Electronic Information, Xiangtan University, Xiangtan* 411105, *China*
[2] *School of Physics and Optoelectronics, Xiangtan University, Xiangtan* 411105, *China*

(Received 4 March 2022; revised manuscript received 28 March 2022; accepted manuscript online 11 April 2022)

Considering the fact that memristors have the characteristics similar to biological synapses, a fractional-order multistable memristor is proposed in this paper. It is verified that the fractional-order memristor has multiple local active regions and multiple stable hysteresis loops, and the influence of fractional-order on its nonvolatility is also revealed. Then by considering the fractional-order memristor as an autapse of Hindmarsh–Rose (HR) neuron model, a fractional-order memristive neuron model is developed. The effects of the initial value, external excitation current, coupling strength and fractional-order on the firing behavior are discussed by time series, phase diagram, Lyapunov exponent and inter spike interval (ISI) bifurcation diagram. Three coexisting firing patterns, including irregular asymptotically periodic (A-periodic) bursting, A-periodic bursting and chaotic bursting, dependent on the memristor initial values, are observed. It is also revealed that the fractional-order can not only induce the transition of firing patterns, but also change the firing frequency of the neuron. Finally, a neuron circuit with variable fractional-order is designed to verify the numerical simulations.

Keywords: fractional-order, multistable, neuron, firing, locally-active memristor

PACS: 05.45.Pq, 87.19.ll, 87.19.lj **DOI:** 10.1088/1674-1056/ac65f7

1. Introduction

As an important basic unit of the nervous system, biological neuron has rich and complex firing activities. In order to study the firing patterns and operating mechanisms of the biological neurons, many neuron models have been proposed based on the experimental data of electrophysiology in recent years. The classic paradigm is the Hodgkin Huxley (HH) model[1] proposed by British physiologist and biophysicist Hodgkin and Huxley in 1952. Subsequently, some simplified models, such as Hindmarsh–Rose (HR),[2] FitzHugh–Nagumo (FHN),[3] Izhikevich,[4] and Morris–Lecar (ML) models[5] were derived from the classic HH model. After that, complex firing activities, which are similar to the dynamics of the biological neurons, have been uncovered in these classical neuron models.[6–10] Synapses are key parts of functional connection and information transmission between neurons. There is a special type of synaptic structure called autapse, which is the synaptic connection formed by axons of neuron and its own dendrites or cell body. Activation of autapse can enhance the reactivity of neurons and promote cluster release, which plays a vital role in neuronal signal processing,[11–13] so how to model the function of biological autapse has become an urgent problem. Memristor[14,15] devices are considered to be the optimal solution to simulate biological synapses due to their good biomimetic characteristics[16,17] such as low power consumption, nonvolatile, plasticity and nano size. Thus, considering memristors as synapses or autapses to construct nervous systems has become a hot topic in the field of neurodynamics. For example, Wang *et al.* proposed a cable neural network with autapse connection, and found that under certain external conditions, autapse can further enhance the adaptive ability to external stimuli.[18] Wang *et al.* studied the influence of autapse on the firing mode and dynamic characteristic of the HR neuron, and revealed that the firing mode of neurons can be changed by adjusting the autaptic intensity and the time-delay.[19] References [20–22] also studied the collective dynamic behaviors of multiple neurons which are coupled by memristor-based autapses.

As we all know, fractional calculus is an extension of integral calculus, which can accurately depict the long memory and hereditary properties of dynamical process in the real world. In recent years, fractional calculus has been widely used in physics, biomedicine, biophysics and other fields.[23–25] In neurodynamics, fractional differentiation can predict stimuli, and improve information processing ability.[26] Therefore, the fractional-order neuron models can mimic the electrical activity of biological neuron more reasonably. In Ref. [27], a complex biological system was modeled by fractional operation calculus in a direct and rigorous manner, accurately describing the propagation of subthreshold nerves. In Ref. [26], it was found that the multi-time scale adaptation of single rat neocortical pyramidal neurons could be well simulated by fractional calculus. The study on dynamics of fractional-order neurons has attracted extensive attention. Yun *et al.* found hidden periodic and chaotic bursting in the fractional-order HR neuron model by fast–slow

†Corresponding author. E-mail: lizhijun_320@163.com

© 2023 Chinese Physical Society and IOP Publishing Ltd

analysis.[28] Alidousti *et al.* revealed the different firing patterns of the fractional-order FNH neuron model and the related bifurcation mechanisms were also explored.[29] The dynamics and chaotic synchronization of two fractional-order HR neurons with time delay under electromagnetic radiation were explored by Meng *et al.*[30] Their research results show that the fractional-order has an important influence on the firing patterns. Furthermore, the effects of fractional-order on synchronization of neuronal networks under different external conditions were reported in Refs. [21–33].

Local activity is the origin of complexity.[34] In 2014, Chua proposed the first locally-active memristor.[35] Compared with ideal memristors, the locally-active memristors have more complex nonlinear dynamic characteristics.[36–40] The multi-stability characteristic of the locally-active memristor[41] makes it a good means to study the firing behavior of neurons. Thus, the locally-active memristor based neurons and neuronal networks have been extensively studied in recent years. For example, Li *et al.* constructed a bistable neural network based on the locally-active memristor, and revealed the switching and bifurcation behaviors of firing patterns in the neural network.[42] Lin *et al.* developed an HR neural network based on a tristable locally-active memristor, and found that the proposed neural network produces three multi-stable phenomena with four different firing patterns simultaneously.[43] A model of HR neuron with four-stable locally-active memristor as self-synapses was proposed by Li *et al.* and they found that four stable firing patterns in the proposed neuron can be switched freely by selecting appropriate initial conditions.[44] With the further development of memristor research, fractional-order locally-active memristors are developed. For example, Xie *et al.* proposed a fractional-order memristor with infinite locally-active interval and coupled it to Chen's chaotic system. They found that the system presents different states under different fractional orders.[45] However, up to now, few studies have been carried out on fractional neuron models with locally-active memristors as autapses.

Inspired by the above studies, a fractional-order multistable locally-active memristor is proposed in this paper, and a neuron model is developed by regarding the proposed locally-active memristor as the autapse of a fractional-order HR neuron. The main contributions of this work are summarized as follows. Firstly, a fractional-order locally-active memristor is developed. Its nonvolatile memory and locally-active characteristics, initial value-dependent coexisting pinched hysteresis loops and fractional-order-dependent electrical behavior are analyzed. Secondly, firing activities of the fractional-order memristive neuron model under different external conditions are studied. Finally, a neuron circuit with variable fractional-order is proposed and the circuit simulation verification is performed.

The layout of this paper is as follows. In Section 2, a fractional-order tristable locally-active memristor is introduced and its related characteristics are studied in detail. In Section 3, a 4D fractional-order neuron model, by considering the fractional-order locally-active memristor as the autapse of 3D-HR neuron, is proposed, and the stability of the neuron model is analyzed. In Section 4, the influences of coupling strength, external excitation current and fractional-order on the firing activities of the fractional-order neuron model are discussed. In Section 5, the circuit simulation of the proposed fractional-order neuron model is carried out, and the conclusion is given in the last section.

2. Model and characteristics of fractional-order multistable memristor

It is well known that there are three definitions for fractional calculus, i.e., Grünwald–Letnikov (GL) definition, Riemann–Liouville (RL) definition and Caputo definition. Among them, Caputo definition is very suitable for real world applications due to its initials with the same form as those of its integer order counterparts. In this paper, the Caputo definition, thus, is used to characterize the neuron model and the Caputo definition of $f(t)$ is described as

$$D_t^{\alpha} f(t) = \begin{cases} \dfrac{1}{\Gamma(n-\alpha)} \displaystyle\int_0^t \frac{f^{(n)}(\tau)}{(t-\tau)^{\alpha-n+1}} \mathrm{d}\tau, & n-1 < \alpha < n, \\ \dfrac{\mathrm{d}^n}{\mathrm{d}^n t} f(t), & \alpha = n, \end{cases} \tag{1}$$

where $0 < \alpha < 1$ is the fractional-order, n is the first integer which is not less than α and $\Gamma(\cdot)$ is the Euler gamma function.

2.1. Fractional-order multistable memristor model

In this paper, a fractional-order multistable locally-active memristor is proposed, which is defined by the state-dependent Ohm's law

$$i = G(\varphi)v = n\varphi v, \tag{2}$$

where i and v represent the input current and input voltage, φ is the internal state variable and $G(\varphi) = n\varphi$ is the defined memductance function. The corresponding state equation can be described as

$$D_t^{\alpha}\varphi = (\mathrm{sgn}(\varphi+2) + \mathrm{sgn}(\varphi-2) - 0.5\varphi) + \beta v, \tag{3}$$

where β is the memristive parameter. It is worth noting that the fractional-order state equation is constructed with sign functions, which are related to the internal state φ and the terminal voltage v. Compared with the existing locally-active memristors whose state equations are implemented with polynomial

functions,[36,38,39] the proposed fractional-order locally-active memristor is more convenient for circuit implementation with low cost. In the following, we study the basic characteristics of the memristor from the aspects of pinched hysteresis loop, nonvolatile memory and locally-active characteristics.

2.2. Pinched hysteresis loop

A pinched hysteresis loop is one of the important characteristics of memristor. When the parameter $\beta = 0.2$ and the order $\alpha = 0.9$, a sinusoidal voltage $v = A\sin(2\pi Ft)$ with amplitude $A = 2$ is applied to the memristor, and the pinched hysteresis loops with different excited frequencies are shown in Fig. 1(a). It can be seen from Fig. 1(a) that when the input frequency F increases from 0.314 to 31.4, the lobe area of the pinch hysteresis loop gradually decreases and finally shrinks into a straight line at $F = 31.4$, resulting in that the memristor degenerates into a fixed resistance.

In addition, when $A = 2$ and $F = 0.314$ remain unchanged, three stable pinched hysteresis loops can be obtained under different initial states $\varphi_0 = -4$, 0, and 4, as shown in Fig. 1(b). In order to study the influence of fractional-order α on the pinched hysteresis loop, keep $A = 2$, $F = 3.14$, and memristor initial value $\varphi_0 = 0$, the fractional-order α is selected as 0.98, 0.9, 0.8, 0.7, and 0.5, respectively, and the hysteresis loops of the memristor are shown in Fig. 1(c). It is observed that the smaller the fractional-order is, the larger the lobe area of the hysteresis loop is, and thus the better memory of the memristor is.[46]

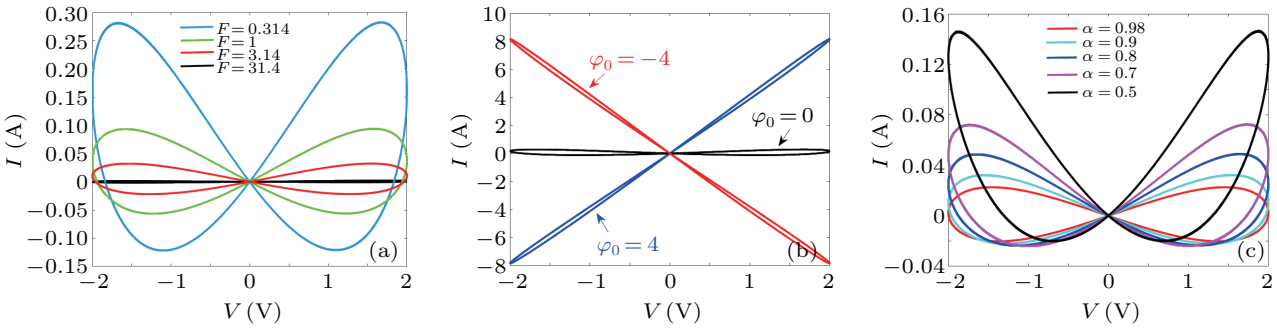


Fig. 1. Pinched hysteresis loops. (a) Hysteresis loops with respect to different frequencies. (b) Initial value dependent pinched hysteresis loops, and (c) fractional-order dependent pinched hysteresis loops.

2.3. Nonvolatile memory and locally-active characteristics

Nonvolatility is also a key feature of the memristor, meaning that it can maintain its latest memductance value even after the applied power is removed. Usually, the power-off plot (POP) is used to judge whether an electronic device is nonvolatile. Let the input voltage $v = 0$, and the state Eq. (3) becomes

$$D_t^\alpha \varphi = \mathrm{sgn}(\varphi + 2) + \mathrm{sgn}(\varphi - 2) - 0.5\varphi. \tag{4}$$

When $\alpha = 0.9$, the POP of the fractional memristor is shown in Fig. 2(a). It can be seen from Fig. 2(a) that the POP has five intersections with the x-axis, among which three intersections $E_1(-4,0)$, $E_3(0,0)$, and $E_5(4,0)$ are negative slope intersections and the other two intersections $E_2(-2,0)$ and $E_4(2,0)$ have an infinite positive slope. The arrows near the intersections in Fig. 2(a) indicate the moving direction of the POP. It is easy to know that the three negative slope intersections are stable equilibrium points and the others two positive slope intersections are unstable equilibrium points. The proposed memristor, thus, can exhibit three stable states, which are dependent on the initial values ϕ_0, namely,

$$\begin{cases} \varphi = \varphi(E_1) = -4, & \varphi(0) < -2, \\ \varphi = \varphi(E_3) = 0, & -2 < \varphi(0) < 2, \\ \varphi = \varphi(E_5) = 4, & 2 < \varphi(0). \end{cases} \tag{5}$$

When $n = 1$, the corresponding memductance values are

$$\begin{cases} w(\varphi(E_1)) = \varphi(Q_1) = -4, & \varphi(0) < -2, \\ w(\varphi(E_3)) = \varphi(Q_3) = 0, & -2 < \varphi(0) < 2, \\ w(\varphi(E_5)) = \varphi(Q_5) = 4, & 2 < \varphi(0). \end{cases} \tag{6}$$

Thus, the proposed memristor is nonvolatile and it acts as a discrete memory device, which can encode three memory states.

DC V–I curve is an important tool to judge whether the memristor has local activity. When the DC V–I curve of the memristor has a negative slope, it is locally-active.[47] Let $D_t^\alpha \varphi = 0$, Eqs. (2) and (3) can be written as

$$V = (\mathrm{sgn}(\phi - 2) - \mathrm{sgn}(\phi + 2) - 0.5\phi), \tag{7}$$

$$I = V\phi = \phi(\mathrm{sgn}(\phi - 2) - \mathrm{sgn}(\phi + 2) - 0.5\phi), \tag{8}$$

where V and I denote DC voltage and current, respectively, and Φ is a variable equilibrium state which satisfies $D_t^\alpha \varphi = (\varphi = \Phi) = 0$. By virtue of Eqs. (6) and (7), the DC V–I curve of the memristor is obtained and shown in Fig. 2(b). As can be seen from Fig. 2(b), there are three negative slope curves of red, green, and blue, which indicates that the memory resistor has three local active regions. That is, the fractional-order memristor is locally active and is suitable for realizing electronic synapse.

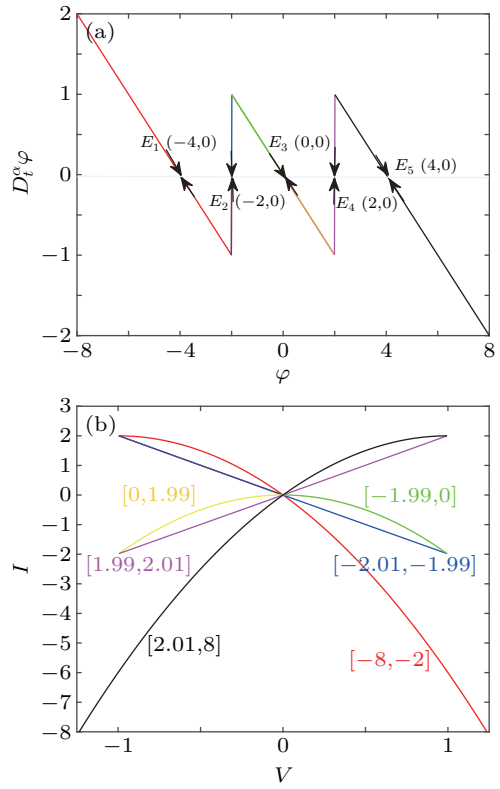


Fig. 2. (a) The power-off-plot (POP) and (b) the DC V–I curve of the locally active memristor.

3. Fractional-order memristive neuron model and its stability analysis

3.1. Fractional-order memristive HR model

According to the Caputo definition, the fractional-order HR neuron model can be described as the following differential equations:

$$\begin{aligned} D_t^\alpha x &= y - ax^3 + bx^2 - z + I, \\ D_t^\alpha y &= c - dx^2 - y, \\ D_t^\alpha z &= r(s(x+1.6) - z), \end{aligned} \tag{9}$$

where x represents the membrane potential, y is the recovery or spiking variable, z is the adaptation variable, I is an external excitation current, α is the system order and a, b, c, d, r, s are system parameters. In this study, we consider the proposed locally-active memristor governed by Eqs. (2) and (3) as an autapse of the fractional-order HR neuron (9), then a 4D neuron model is developed, which is formulated as

$$\begin{aligned} D_t^\alpha x &= y - ax^3 + bx^2 - z + I + k\varphi x, \\ D_t^\alpha y &= c - dx^2 - y, \\ D_t^\alpha z &= r(s(x+1.6) - z), \\ D_t^\alpha \varphi &= (\mathrm{sgn}(\varphi+2) + \mathrm{sgn}(\varphi-2) - 0.5\varphi) + \beta x, \end{aligned} \tag{10}$$

where k is the coupling strength. In this paper, the parameters are determined as $a=1$, $b=3$, $c=1$, $d=5$, $r=0.0021$, $s=4$, and $\beta=0.2$. The effects of external excitation current I, fractional-order α, and coupling strength k on the firing dynamics of the memristive neuron model are discussed in detail in Section 4.

3.2. Stability analysis of equilibrium points

In order to analyze the stability of the equilibrium point of the fractional-order neuron, the following theorem is introduced.

Lemma 1[48] For a fractional-order system with order $0 < \alpha \le 1$:

$$D_t^\alpha X(t) = f_i(X(t)), \quad X(0) = X_0, \tag{11}$$

where

$$\begin{aligned} X(t) &= (x(t), y(t), z(t), \varphi(t))^{\mathrm{T}}, \\ f(X) &= [f_1(X), f_2(X), f_3(X), f_4(X)]^{\mathrm{T}}, \\ f_i(X) &= (x, y, z, \varphi), \quad (i = 1,2,3,4), \end{aligned}$$

$E(x_0, y_0, z_0, \varphi_0)$ is a fractional-order system equilibrium point. If all the eigenvalues λ_i $(i = 1,2,3,\ldots,n)$ of the Jacobian matrix satisfy the following condition:

$$|\arg(\lambda_i)| > \alpha\pi/2, \quad (i = 1,2,\ldots,n), \tag{12}$$

the equilibrium point is asymptotically stable.

Let the right side of Eq. (10) equal to 0, the equilibrium point of the system can be written as E $(x_0,\ 1-5x_0^2,\ 4(x_0+1.6),\ \varphi_0)$, where x_0 and φ_0 are determined by

$$\begin{aligned} &-x_0^3 - 2x_0^2 + (k\varphi_0 - 4)x_0 + I - 5.4 = 0, \\ &\mathrm{sgn}(\varphi_0+2) + \mathrm{sgn}(\varphi_0-2) - 0.5\varphi_0 + 0.2x_0 = 0. \end{aligned} \tag{13}$$

It can be seen from Eq. (13) that the equilibrium point of the system is related to the external excitation current I and the coupling strength k. The Jacobian matrix of system in Eq. (10) at equilibrium point E is expressed as

$$J_E = \begin{Bmatrix} a & 1 & -1 & kx_0 \\ -10x_0 & -1 & 0 & 0 \\ 0.0084 & 0 & -0.0021 & 0 \\ 0.2 & 0 & 0 & b \end{Bmatrix}, \tag{14}$$

where

$$\begin{aligned} a &= -3x_0^2 + 6x_0 + k\varphi_0, \\ b &= 10^6(1 - \tanh^2(10^3(\varphi_0+2))) \\ &\quad + 10^6(1 - \tanh^2(10^3(\varphi_0-2))) - 0.5. \end{aligned}$$

The characteristic equation of system in Eq. (10) at equilibrium point E is

$$\lambda^4 + A\lambda^3 + B\lambda^2 + C\lambda + D = 0, \tag{15}$$

where

$$A = \frac{10021}{10000} - b - a,$$

$$B = 10x_0 - \frac{10021b}{10000} - \frac{10021a}{10000} + ab - \frac{kx_0}{5} + \frac{21}{2000},$$
$$C = \frac{21x_0}{1000} - \frac{21b}{2000} - \frac{21a}{10000} + \frac{10021ab}{10000} - 10x_0b + \frac{21}{2500} - \frac{10021kx_0}{50000},$$
$$D = \frac{21ab}{10000} - \frac{21b}{2500} - \frac{21x_0b}{1000} - \frac{21kx_0}{50000}.$$

With $k = 0.1$, $I = 2.7$, and other parameters remain unchanged, the two expressions in Eq. (13) can be graphically expressed, as displayed in Fig. 3. As we can see from Fig. 3, two curves govern by Eq. (13) have five intersections, where φ_0 is equal to -2 at the point E_4 and 2 at the point E_5. However, when $\varphi_0 = -2$ or 2, Eq. (13) has no solution, therefore, E_4 and E_5 are not equilibrium points. The system, thus, has three equilibrium points E_1, E_2 and E_3.

In order to discuss the influence of external excitation current I and the fractional-order α on the stability of the equilibrium points, we list the eigenvalues of the three equilibrium points and the relationship between stability and their fractional-order under different external excitation current $I =$ 1.27, 1.5, 1.95, and 2.7, as shown in Table 1. According to Eq. (15), each equilibrium point has four eigenvalues, and the stability of each equilibrium point is judged by Lemma 1.

According to Lemma 1 and Table 1, we can find when the real parts of the eigenvalues of the equilibrium points are all less than 0, the neuron is stable and independent of the fractional-order α. When the eigenvalues of the equilibrium point have both positive real parts and imaginary parts, the stability of the equilibrium point is decided by the fractional-order α. When the eigenvalues of the equilibrium point of the neuron have pure positive real roots, the system is unstable and independent of the fractional-order α.

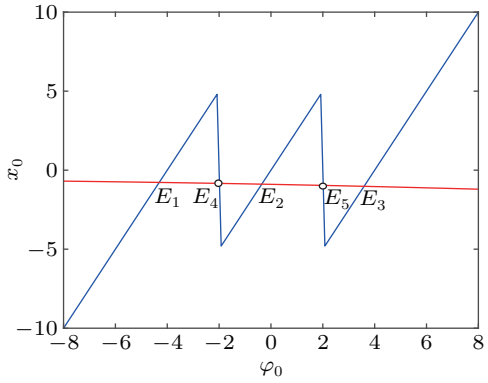


Fig. 3. Two function curves and their intersections, wherein E_1, E_2, and E_3 are equilibrium points, E_4 and E_5 are not equilibrium points.

Table 1. Equilibrium points and their stability when $k = 0.1$.

I	Equilibrium points	Eigenvalues	Stability analysis
1.27	E_1 (−1.1846, −6.0164, 1.6616, −4.4738)	$\lambda_1 = -12.7663$, $\lambda_2 = -0.4981$, $\lambda_{3,4} = 0.0000 \pm 0.0256$i	critical stable
	E_2 (−1.3039, −7.5008, 1.1844, −0.5215)	$\lambda_1 = -14.0598$, $\lambda_2 = -0.4981$, $\lambda_{3,4} = -0.0018 \pm 0.0245$i	stable
	E_3 (−1.4440, −9.4257, 0.624, 3.4223)	$\lambda_1 = -15.5661$, $\lambda_2 = -0.4980$, $\lambda_{3,4} = -0.0076 \pm 0.0226$i	stable
1.5	E_1 (−1.1268, −5.3483, 1.8928, −4.4507)	$\lambda_1 = -12.0333$, $\lambda_2 = -0.4981$, $\lambda_{3,4} = 0.0073 \pm 0.0247$i	$\alpha < 0.817$, stable; $\alpha > 0.817$, unstable
	E_2 (−1.25247, −6.8434, 1.3901, −0.5009)	$\lambda_1 = -13.2876$, $\lambda_2 = -0.4981$, $\lambda_{3,4} = 0.0063 \pm 0.0237$i	$\alpha < 0.835$, stable; $\alpha > 0.835$, unstable
	E_3 (−1.3893, −8.6509, 0.8427, 3.4442)	$\lambda_1 = -14.7872$, $\lambda_2 = -0.4980$, $\lambda_{3,4} = 0.00057 \pm 0.0237$i	$\alpha < 0.984$, stable; $\alpha > 0.984$, unstable
1.95	E_1 (−1.0029, −4.0290, 1.23884, −4.4011)	$\lambda_1 = -10.5250$, $\lambda_2 = -0.4982$, $\lambda_{3,4} = 0.0231 \pm 0.0128$i	$\alpha < 0.322$, stable; $\alpha > 0.322$, unstable
	E_2 (−1.1270, −5.3506, 1.8920, −0.4508)	$\lambda_1 = -11.6709$, $\lambda_2 = -0.4982$ $\lambda_{3,4} = 0.0247 \pm 0.0000$i	critical unstable
	E_3 (−1.2674, −7.0315, 1.3304, 3.4931)	$\lambda_1 = -13.1173$, $\lambda_2 = -0.4981$, $\lambda_{3,4} = 0.0197 \pm 0.0129$i	$\alpha < 0.369$, stable; $\alpha > 0.369$, unstable
2.7	E_1 (−0.7755, −2.0073, 3.2977, −4.3102)	$\lambda_1 = -7.9944$, $\lambda_2 = -0.4982$ $\lambda_3 = 0.0929$, $\lambda_4 = 0.00897$	unstable
	E_2 (−0.5556, −2.9221, 2.8572, −0.3542)	$\lambda_1 = -8.8307$, $\lambda_2 = -0.4983$, $\lambda_3 = 0.1183$, $\lambda_4 = 0.0058$	unstable
	E_3 (−1.02219, −4.2244, 2.3112, 3.5911)	$\lambda_1 = -10.0368$, $\lambda_2 = -0.4983$, $\lambda_3 = 0.11956$, $\lambda_4 = 0.00478$	unstable

4. Dynamic analysis

In order to study the dynamic behaviors of the neuron, nonlinear dynamical analysis tools such as time series, phase diagram, bifurcation diagram, Lyapunov exponent and ISI bifurcation diagram are used to analyze the firing activities. In the process of numerical analysis, the system parameters are fixed as $a = 1$, $b = 3$, $c = 1$, $d = 5$, $r = 0.0021$, $s = 4$, and $\beta = 0.2$. It should be noted that the Adomian fractional-order algorithm[49] is adopted in this paper, the step length of simulation is $h = 0.01$, the computing software used is Matlab2019b, and the computer system is based on the Win10 home edition.

What needs special attention is that many studies have shown that autonomous and non-autonomous fractional-order systems do not have any exact periodic solution.[50,51] However, when the trajectory of a fractional-order system satisfies $\lim_{t\to\infty} x_i(t+T) - x_i(t) = 0$, $i = 1, 2, 3, \ldots, n$, for $T > 0$, according to Ref. [52], this phenomenon is named asymptotically T-periodic oscillations. Some studies have shown that there exist asymptotically periodic oscillations in the fraction-order circuits and systems.[45,52–54] In this paper, we also find the existence of asymptotically periodic oscillations in the proposed fractional-order neuronal model. To facilitate recording, the term "asymptotically periodic" is written as "A-periodic" in

the following.

4.1. Coexisting firing behavior

In order to explore the coexisting firing behavior of the fractional-order neuron model, the system parameters are fixed as $k = 0.1$, $\alpha = 0.9$, $I = 2.7$, and $\beta = 0.2$, the initial values of the fractional-order neuron model are (1, 0, 0, −4), (1, 0, 0, 0), and (1, 0, 0, 4). The corresponding time series of the membrane potential x are shown in the Figs. 4(a)–4(c) respectively. From Figs. 4(a) and 4(b), we know that $\lim_{t\to t_1} x_i(t+T) - x_i(t) = 0$ and $\lim_{t\to t_2} x_i(t+T) - x_i(t) = 0$ are established and the neuron has two A-periodic solutions. Although they are both A-periodic solutions, they exhibit different firing patterns. As illustrated in Fig. 4(a), the neuron exhibits irregular A-periodic bursting oscillations, in which the repetitive firing amplitude decreases gradually until it disappears in each burster.[55] While in Fig. 4(b), the system shows A-periodic bursting oscillations, in which there exist seven firing pulses with approximately equal amplitude in each burster. However, when the initial value of the fractional neuron model is (1, 0, 0, 4), no period T satisfies $\lim_{t\to t_3} x_i(t+T) - x_i(t) = 0$, and thus, the neuron shows a chaos oscillation state, as shown in Fig. 4(c). From Fig. 4(d), we find the neuron model can exhibit three distinct firing patterns under different initial values.

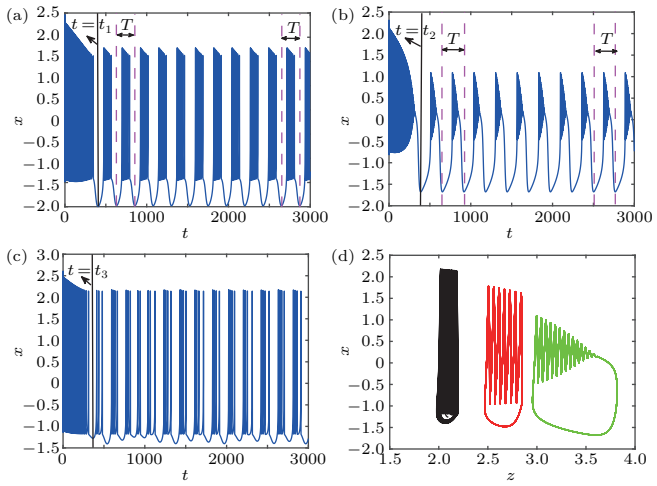


Fig. 4. Firing patterns of the fractional-order neuron. (a)–(c) Time series of the membrane potential x with the initial values (1, 0, 0, −4), (1, 0, 0, 0), and (1, 0, 0, 4), respectively. (d) Phase diagrams, where black, red, and green respectively represent the initial value of (1, 0, 0, −4), (1, 0, 0, 0), and (1, 0, 0, 4)).

In order to verify the above three different firing patterns, the initial value φ_0 of the memristor is considered as the controlled parameter and the others parameters remain unchanged. The bifurcation diagram and Lyapunov exponents with respect to the initial value φ_0 are obtained in Figs. 5(a) and 5(b), respectively. For clarity, the others two Lyapunov exponents LE3 and LE4 in Fig. 5(b) are neglected since their values are much less than 0. When the initial value φ_0 locates at the region of (−6, −2) and (−2, 2), the system is A-periodic. While when the initial value φ_0 is in the region of (2, 6), the system presents a chaotic state. From Fig. 5(b), we can find that the maximum Lyapunov exponent is approximately equal to 0 when the initial value φ_0 locates at (−6, 2) and (−2, 2), meaning the neuron is in an A-periodic oscillation state; while the maximum Lyapunov exponent is greater than 0 when the range of initial value φ_0 is (2, 6), showing that the neuron produces chaotic oscillation behavior. So, the bifurcation diagram and the Lyapunov exponents are well consistent.

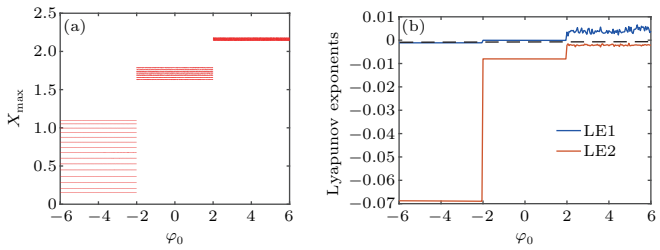


Fig. 5. (a) Bifurcation diagram of x with memristor initial value φ_0. (b) Lyapunov exponents with memristor initial value φ_0.

4.2. Influence of excitation current

In the real world, neurons respond differently to different external stimuli. In this part, we discuss the effect of the excitation current I on the fractional neuron model. Keep $\alpha = 0.9$, $k = 0.1$, $\beta = 0.2$ and the initial value of the system as (1, 0, 0, 4), when the external excitation current I changes from 1.4 to 3.1, the ISI bifurcation diagram and Lyapunov exponents[56,57] are shown in Figs. 6(a) and 6(b), respectively. Similarly, the others two Lyapunov exponents LE3 and LE4 are neglected because their values are much less than 0.

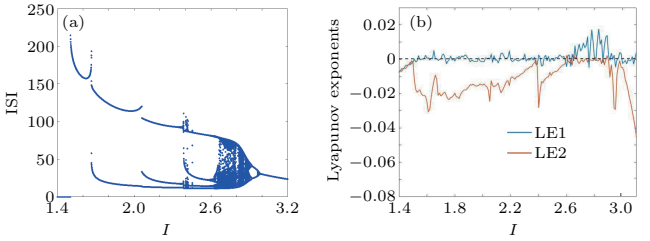


Fig. 6. (a) ISI bifurcation diagram and (b) Lyapunov exponents with respect to the external excitation current I.

In a fractional-order system, if the trajectory of the system is A-periodic oscillation in some intervals, while the trajectory of other adjacent regions is chaotic, this phenomenon is called "local chaos".[42] From Fig. 6(a), as the external excitation current I increases from 1.5 to 2.6, the firing frequency of the fractional-order neuron gradually increases from A-periodic-1 to A-periodic-4. When I increases from 2.6 to 3.1, the neuron appears an A-periodic–chaos–A-periodic switching process. Namely, the neuron presents local chaos. The Lyapunov exponents shown in Fig. 6(b) also verify the effect of the external excitation current I on firing activity of neuron model.

4.3. Influence of coupling strength

Set the fractional-order $\alpha = 0.9$, $\beta = 0.2$, $I = 2.7$, and the initial value of the system is (1, 0, 0, 0). The coupling strength k is considered as the controlled parameter to explore its influence on the firing dynamics of the neuron model. When the coupling strength k increases from 0.1 to 1.4, the ISI bifurcation diagram and the corresponding Lyapunov exponents are illustrated in Figs. 7(a) and 7(b), respectively. From Figs. 7(a) and 7(b), when coupling strength $k \in (0, 0.5)$, the system is in an A-periodic state; when coupling strength $k \in (0.5, 0.95)$, the system alternates between A-periodic and chaotic states. As the coupling strength k increases from 0.95 to 1.4, the neuron undergoes a series of inverse period doubling bifurcations and finally shows A-period 1 oscillations.

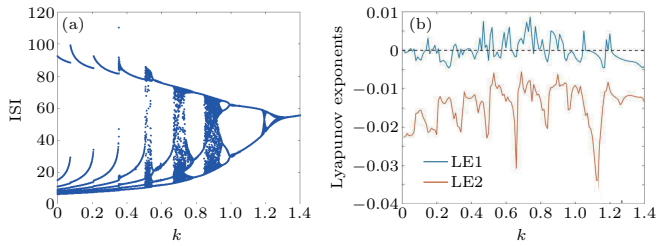


Fig. 7. The effect of the coupling strength on firing patterns. (a) ISI bifurcation diagram and (b) Lyapunov exponents. The initial value is (1, 0, 0, 0) and $I = 2.7$, $\alpha = 0.9$.

4.4. Influence of fractional-order

The firing frequency of neuron has great influence on the transmission and processing of neural signals. The more spikes in per unit of time, the action and the firing frequency of neuron will become faster. In order to study the effect of the fractional-order α on the firing frequency of the fractional-order neuron model, set $k = 0.1$, $\beta = 0.2$, $I = 2.7$, and the fractional-order α varies from 0.55 to 1. The ISI bifurcation diagram of the fractional neuron with the initial value of (1, 0, 0, 4) is shown in Fig. 8.

From Fig. 8, when α increases from 0.55 to 0.7, the neuron exhibits A-periodic firing and the ISI of the neuron increases gradually, meaning the firing frequency decreases gradually. Figures 9(a) and 9(b) illustrate the time series of the membrane potential x with the fractional-order $\alpha = 0.6$ and 0.68, respectively. In the duration of $t = (1000, 1200)$, Fig. 9(a) contains 6 complete A-periodic oscillations, while there are just 4 complete A-periodic oscillations in Fig. 9(b). So, we can intuitively observe that the firing frequency decreases as the increase of the fractional-order α.

However, from Fig. 8, as the fractional-order α increases from 0.7 to 1, the firing pattern of the neuron changes from A-periodic to chaotic firing. In order to verify the transition of firing pattern, the time series of the membrane potential x with $\alpha = 0.7$ and 0.8 are provided in Figs. 10(a) and 10(b), respectively. And the corresponding phase diagrams are shown in Figs. 10(c) and 10(d). It is easy to find when the fractional-order is 0.7, the neuron exhibits A-periodic 5 oscillation, while for $\alpha = 0.8$, the neuron is in chaotic oscillation state.

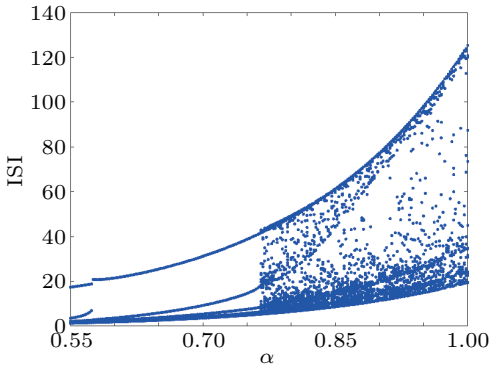


Fig. 8. Inter spike interval (ISI) bifurcation diagram with fractional-order α.

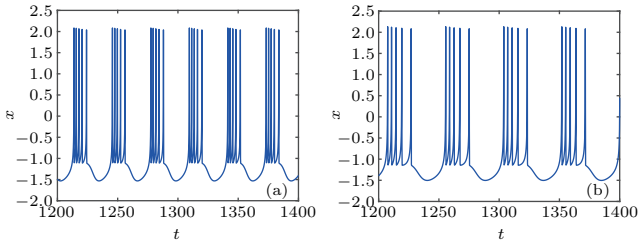


Fig. 9. The membrane potential with different orders. (a) $\alpha = 0.6$, (b) $\alpha = 0.68$.

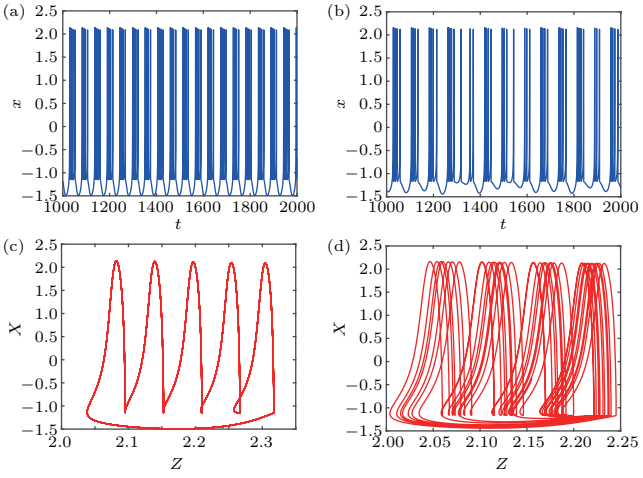


Fig. 10. Firing patterns with respect to the fractional-order α. The initial value of the neuron is (1, 0, 0, 4), $I = 2.7$ and $k = 0.1$. (a) and (b) The time series of the membrane potential with $\alpha = 0.7$ and $\alpha = 0.8$, respectively, (c) and (d) The corresponding phase diagrams.

5. Circuit simulations

5.1. Schematics and circuit parameter selections

In this section, the memristive autapse coupling neuron model governed by Eq. (10) is realized by using the off-the-shelf electronic components, as shown in Fig. 11, in which the operational amplifiers TL082CD and the analog multipliers AD633AN are biased with ± 15 V voltage. From Fig. 11, the complete system circuit consists of three modules: memristor module, α order module and neuron module. It should

be noted that the M above the operational amplifier represents the fractional-order capacitor. According to the Kirchhoff's current law, the circuit shown in Fig. 11 can be described by the following equations:

$$\begin{aligned}
\tau_1 \frac{\mathrm{d}^\alpha V_x}{\mathrm{d}t^\alpha} &= \frac{R_7}{R_8}V_y + \frac{g_1 R_7}{R_9}V_x^2 - \frac{g_1 g_2 R_7}{R_{10}}V_x^3 \\
&\quad - \frac{R_7}{R_{11}}V_z + \frac{R_7}{R_a}V_1 + \frac{R_7}{R_b}V_x V_\varphi, \\
\tau_2 \frac{\mathrm{d}^\alpha V_y}{\mathrm{d}t^\alpha} &= \frac{R_{12}}{R_{13}}V_2 - \frac{g_3 R_{12}}{R_{140}}V_x^2 - \frac{R_{12}}{R_{15}}V_y, \\
\tau_3 \frac{\mathrm{d}^\alpha V_z}{\mathrm{d}t^\alpha} &= \frac{R_{16}}{R_{17}}V_x + \frac{R_{16}}{R_{18}}V_3 - \frac{R_{16}}{R_{19}}V_z, \\
\tau_3 \frac{\mathrm{d}^\alpha V_\varphi}{\mathrm{d}t^\alpha} &= \frac{R_1}{R_2}\left(\frac{13.5R_\mathrm{f}\cdot \mathrm{sgn}(V_\varphi + 2)}{R_3}\right. \\
&\quad \left. + \frac{13.5R_\mathrm{f}\cdot \mathrm{sgn}(V_\varphi + 2)}{R_4} - \frac{R_\mathrm{f} V\varphi}{R_5}\right) + \frac{R_1}{R_6}V_x, \quad (16)
\end{aligned}$$

where four state variables V_x, V_y, V_z, and V_φ, denote capacitor voltages of four integral circuit channels, respectively, and $\tau_1 = \tau_2 = \tau_3 = \tau_4 = R_0 C_0$ are time constants of each channel. Comparing the dynamical Eq. (16) with the neuron model Eq. (10), when the circuit parameters and system parameters satisfy the following relations:

$$\begin{aligned}
&\frac{R_7}{R_8} = 1, \quad \frac{g_1 R_7}{R_9} = a, \quad \frac{g_1 g_2 R_7}{R_{10}} = b, \quad \frac{R_7}{R_{11}} = 1, \\
&\frac{R_7}{R_a}V_1 = I, \quad \frac{R_7}{R_b} = k, \quad \frac{R_{12}}{R_{13}}V_2 = c, \quad \frac{g_3 R_{12}}{R_{14}} = d, \\
&\frac{R_{12}}{R_{15}} = 1, \quad \frac{R_{16}}{R_{17}} = rs, \quad \frac{R_{16}}{R_{18}}V_3 = 1.6rs, \quad \frac{R_{16}}{R_{19}} = r, \\
&\frac{R_1}{R_2}\frac{13.5R_\mathrm{f}}{R_3} = 1, \quad \frac{R_1}{R_2}\frac{13.5R_\mathrm{f}}{R_4} = 1, \quad \frac{R_\mathrm{f}}{R_5} = 0.5, \quad \frac{R_1}{R_6} = \beta,
\end{aligned}$$

then the circuit Eqs. (16) are equivalent to those of Eq. (10). The proposed circuit can simulate the firing dynamics of the fractional-order neuron. Fixing the system parameters as $a = 1$, $b = 3$, $c = 1$, $d = 5$, $r = 0.0021$, $s = 4$, $\beta = 0.2$, $k = 0.1$ and letting $\tau_1 = \tau_2 = \tau_3 = \tau_4 = 100$, we can obtain the following specific values of the circuit parameters: $g_1 = g_3 = g_4 = 1$, $R_0 = 10$ kΩ, $C_0 = 1$ μF, $R_\mathrm{a} = R_1 = R_7 = R_8 = R_9 = R_{11} = R_{12} = R_{13} = R_{15} = R_{16} = 10$ kΩ, $R_\mathrm{b} = 100$ kΩ, $R_6 = 50$ kΩ, $R_\mathrm{f} = 1$ kΩ, $R_3 = R_4 = 13.5$ kΩ, $R_5 = 2$ kΩ, $R_{10} = 1$ kΩ, $R_{14} = 2$ kΩ, $R_{17} = 1190.47$ kΩ, $R_{18} = 744.047$ kΩ, $R_{19} = 4761.9$ kΩ, $R_{20} = 10$ kΩ, $V_1 = V_2 = V_3 = 1$ V.

According to Ref. [58], the equivalent expression of α-order capacitor in complex frequency domain can be written as

$$F(s) = \frac{R_1}{sR_1C_1 + 1} + \frac{R_2}{sR_2C_2 + 1} + \cdots + \frac{R_n}{sR_nC_n + 1}, \quad (17)$$

where n is the number of unit integrating units. When fractional-order capacitors with $\alpha = 0.7$, 0.8, 0.9, and 0.98, according to Refs. [59,60], we can obtain the following expressions:

$$F(s) = \begin{cases}
\dfrac{R_1}{sR_1C_1 + 1} + \dfrac{R_2}{sR_2C_2 + 1} + \dfrac{R_3}{sR_3C_3 + 1} + \dfrac{R_4}{sR_4C_4 + 1} + \dfrac{R_5}{sR_5C_5 + 1} + \dfrac{R_6}{sR_6C_6 + 1}, & \alpha = 0.7, \\
\dfrac{R_1}{sR_1C_1 + 1} + \dfrac{R_2}{sR_2C_2 + 1} + \dfrac{R_3}{sR_3C_3 + 1} + \dfrac{R_4}{sR_4C_4 + 1} + \dfrac{R_5}{sR_5C_5 + 1}, & \alpha = 0.8, \\
\dfrac{R_1}{sR_1C_1 + 1} + \dfrac{R_2}{sR_2C_2 + 1} + \dfrac{R_3}{sR_3C_3 + 1}, & \alpha = 0.9, \\
\dfrac{R_1}{sR_1C_1 + 1} + \dfrac{R_2}{sR_2C_2 + 1}, & \alpha = 0.98.
\end{cases} \quad (18)$$

The corresponding resistance and capacitance values with different fractional-order α are listed in Table 2. In the fractional-order capacitor module, the switching elements are used to realize different fractional-orders. For example, when the switch K_1 is closed and the others switches are turned off, M is a fractional-order capacitor with $\alpha = 0.98$. In this way, we can obtain other three fractional-order capacitors.

Table 2. The resistance and capacitance values of the α-order capacitors.

α	R_1 (Ω)	R_2 (Ω)	R_3 (Ω)	R_4 (Ω)	R_5 (Ω)	R_6 (Ω)	C_1 (μF)	C_2 (μF)	C_3 (μF)	C_4 (μF)	C_5 (μF)	C_6 (μF)
0.7	2.19×10^7	2.60×10^6	5.26×10^5	1.13×10^4	2.46×10^4	6.00×10^3	3.284	3.139	1.700	0.886	0.454	0.207
0.8	3.79×10^7	1.75×10^6	1.70×10^5	1.70×10^4	1.80×10^3	–	1.980	2.400	1.390	0.780	0.420	–
0.9	6.284×10^7	2.50×10^5	2.50×10^2	–	–	–	1.232	1.835	1.1	–	–	–
0.98	9.12×10^7	1.91×10^2	–	–	–	–	0.975	3.681	–	–	–	–

5.2. Circuit simulation results

Referring to the circuit schematic diagram provided in Fig. 11, the fractional-order memristive HR neuron circuit is designed based on the Multisim 14.0. According to the voltage dividing principle of shunt capacitor, the initial voltage of shunt capacitor is equal to the sum of all shunt capacitors. For the convenience of design, only the initial value of the capacitor C_1 is changed and the initial values of the others capacitors

are set to 0 in the fractional-order capacitor module.

Firstly, we simulate the electrical behavior of the fractional-order memristor by using Multisim 14.0. Closing K_2 so that the fractional-order $\alpha = 0.9$, applying a sinusoidal voltage with amplitude $A = 2$ V and frequency $F = 3.14$ Hz to the fractional-order memristor, we obtain three stable pinched hysteresis loops with different initial values. As illustrated in Fig. 12(a), the red, green, and blue hysteresis loops are related to $V_{C1} = 4$ V, 0 V, and -4 V, respectively. Thus, the circuit simulation results effectively verify the numerical simulation results shown in Fig. 1(b), indicating that the proposed fractional-order memristor can indeed exhibit the coexisting hysteresis loops. Let $V_{C1} = 0$ V, and close K_4, K_3, K_2, and K_1 sequentially, the corresponding pinched hysteresis loops corresponding to different fractional-orders are provided in Fig. 12(b), which are similar as the numerical simulation results illustrated in Fig. 1(c).

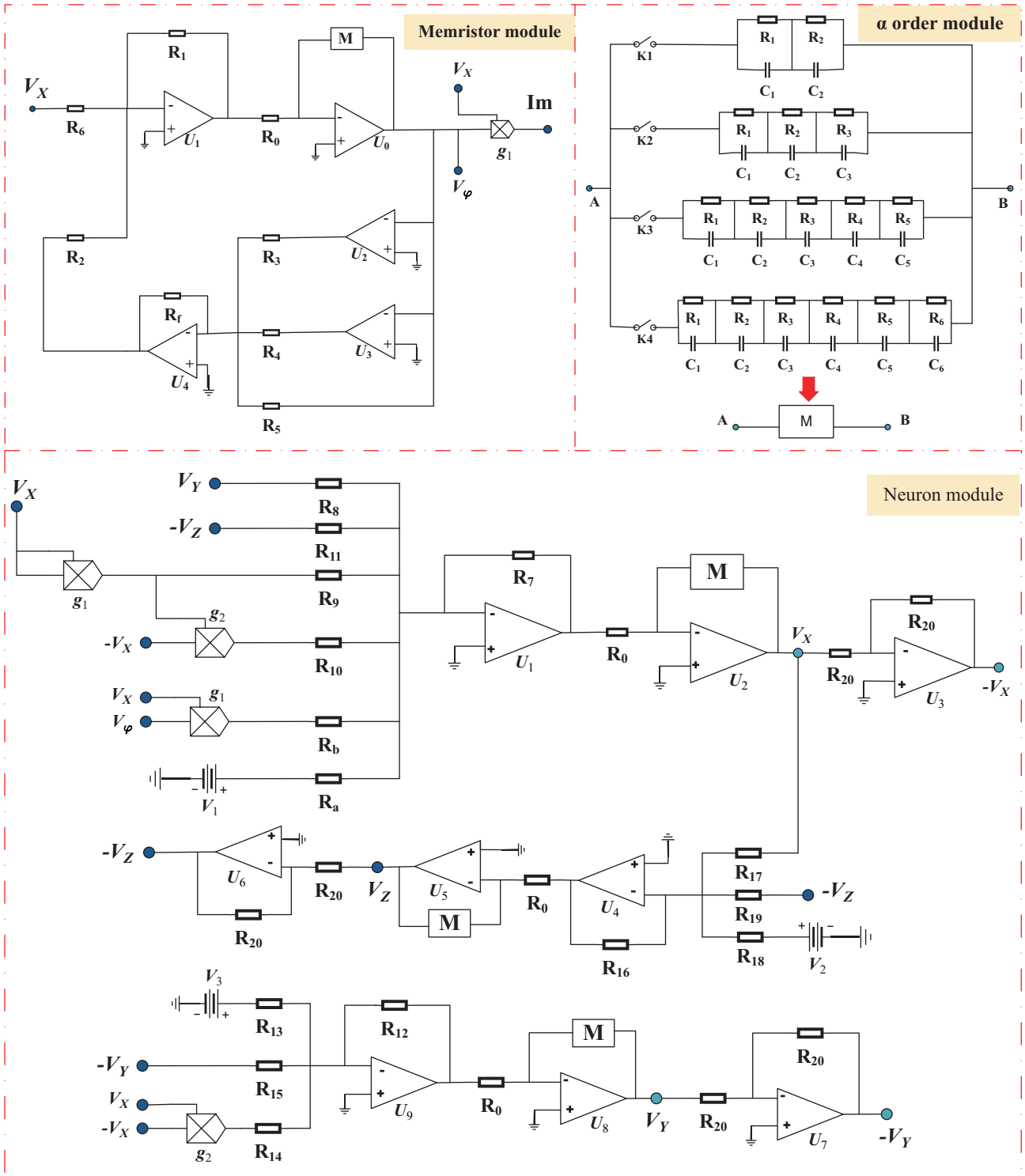


Fig. 11. The main circuit of fractional-order neuron model including memristor module, α order module and neuron module.

Secondly, the coexisting firing patterns of the memristive neuron are also verified by Multisim circuit simulation. Close K_2 so that the fractional-order $\alpha = 0.9$, let $V_{C1} = -4$ V, 0 V, and 4 V, respectively, the corresponding time series of the membrane potential x with different initial values are shown in Figs. 13(a)–13(c) and the corresponding phase portraits in z–x plane are illustrated in Fig. 13(d). From Fig. 13, we can find that the neuron circuit exhibits three coexisting firing patterns, namely, irregular A-periodic oscillations, A-periodic-7 oscillations and chaotic oscillations, which are well consistent with the numerical simulation results illustrated in Fig. 4.

Finally, the firing activities of the neuron circuit dependent on different fractional-orders are plotted in Fig. 14. For simplicity, we only consider two cases, namely, $\alpha = 0.7$ and $\alpha = 0.8$. When only the switch K_4 is closed, the corresponding fractional-order is $\alpha = 0.7$, we find the neuron circuit exhibits A-periodic bursting with 5 spikes, the corresponding time series and phase diagram are plotted in Figs. 14(b) and 14(a). While K_3 is on, which means $\alpha = 0.8$, we can observe complex chaotic firing activities, as illustrated in Figs. 14(d) and 14(c). From the numerical simulation results in Fig. 10 and the circuit simulation results in Fig. 14, it is easy to find that the fractional-order has an important effect on the firing activities of the memristive neuron.

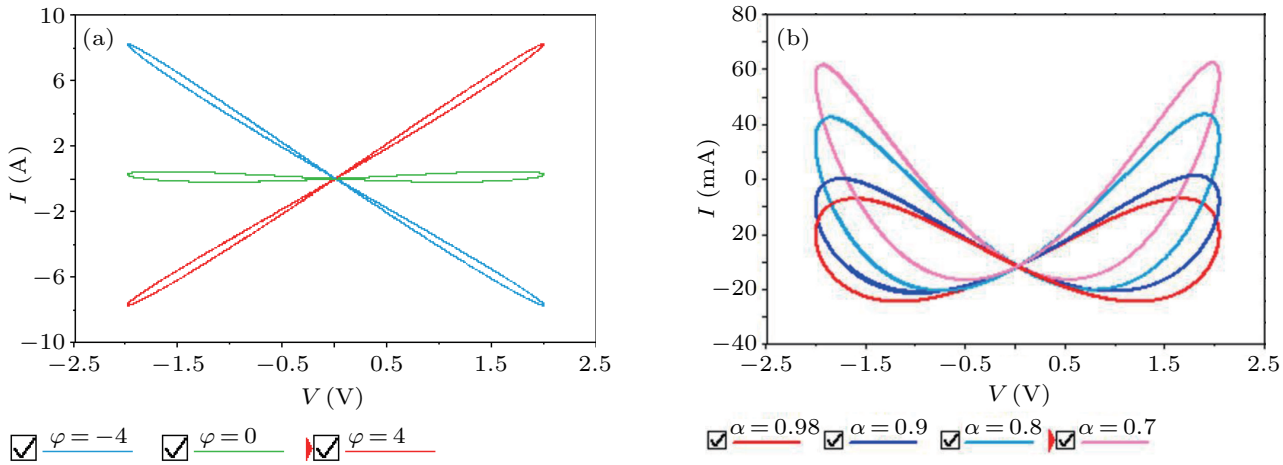


Fig. 12. The pinched hysteresis loops obtained by circuit simulation. (a) Three stable hysteresis loops with different initial values, (b) hysteresis loops with different fractional-orders.

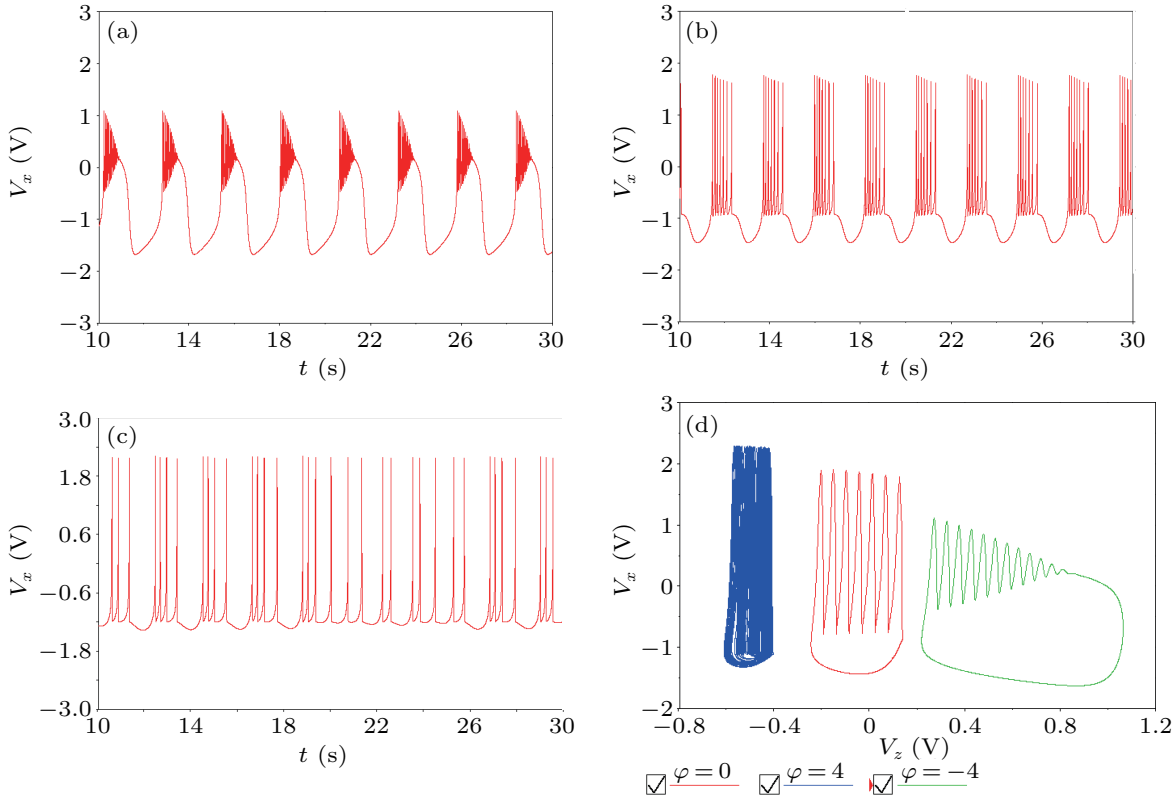


Fig. 13. The coexisting firing patterns in circuit simulation. (a)–(c) The time series of the membrane potential with $V_{C1} = -4$ V, 0 V, and 4 V, respectively, and (d) phase diagram in V_z–V_x plane.

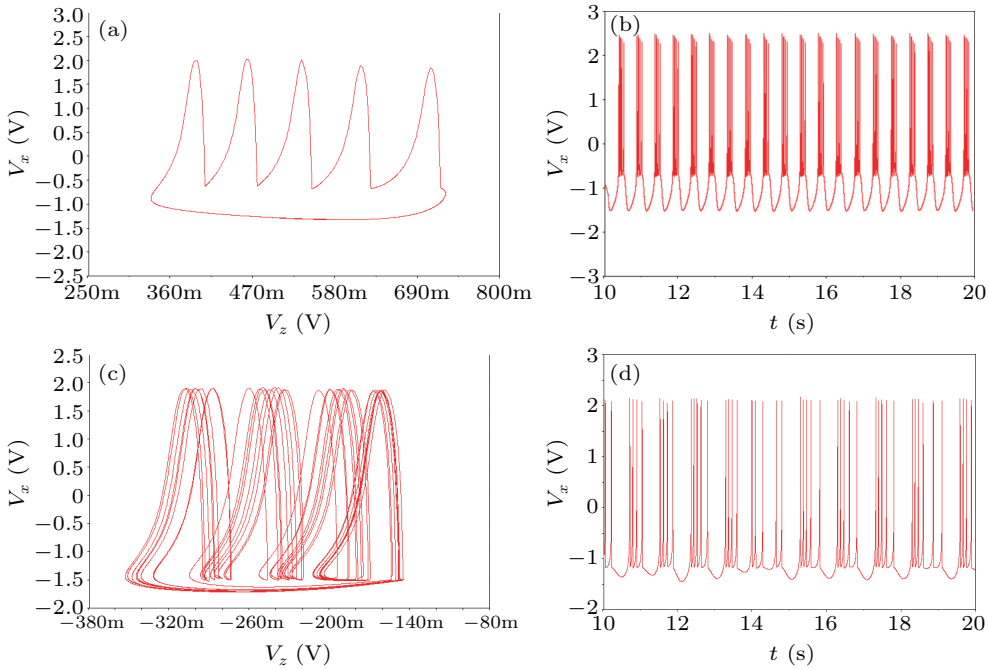


Fig. 14. The fractional-order dependent firing activities. (a) The time series and (b) phase diagram with $\alpha = 0.7$, (c) the time series and (d) phase diagram with $\alpha = 0.8$.

6. Conclusion

In this paper, a multistable fractional-order locally-active memristor is proposed, and its nonvolatile and locally-active characteristics are studied and analyzed. Then, a 4D fractional-order HR neuron model is developed by introducing the designed memristor as an autapse of a fractional-order 3D HR neuron model. The effects of initial value, coupling strength, external excitation current and fractional-order α on the firing activities of the fractional-order neuron model are discussed in detail by numerical and circuit simulations. Some complex firing phenomena including the coexisting firing patterns ignited by different initial values, alternation of A-periodic and chaotic firing induced by coupling strength, are observed. Furthermore, we find that the fractional-order α can not only affect the firing patterns but also change the firing frequency of the neuron. It is expected that this study will be helpful to the theoretical analysis and understanding of the fractional-order locally-active memristor and the firing activities of the fractional-order neuron.

Acknowledgments

Project supported by the National Key Research and Development Program of China (Grant No. 2018AAA0103300) and the National Natural Science Foundation of China (Grant Nos. 62171401 and 62071411).

References

[1] Hodgkin A L and Huxley A F 1952 *J. Physiol.* **117** 500
[2] Hindmarsh J L and Rose R M 1984 *Philos. Trans. R. Soc. Lond B Biol. Sci.* **221** 87
[3] FitzHugh R 1961 *Biophys. J.* **1** 445
[4] Izhikevich E M 2004 *IEEE Trans. Neural Networks* **15** 1063
[5] Morris C and Lecar H 1981 *Biophys. J.* **35** 193
[6] Han F, Wang Z J and Fan H 2015 *Chin. Phys. Lett.* **32** 040502
[7] Ding L X, Jia B and Li Y Y 2019 *Acta Phys. Sin.* **68** 180502 (in Chinese)
[8] Lu Y M, Wang C H and Deng Q L 2022 *Chin. Phys. B* **31** 060502
[9] Qi G and Wang Z 2020 *Chin. Phys. B* **30** 120516
[10] Xu Y, Liu M and Zhu Z 2020 *Chin. Phys. B* **29** 098704
[11] Yin L, Zheng R, Ke W, He Q and Zhang Y 2018 *Nat. Comm.* **9** 4890
[12] Yilmaz E, Ozer M, Baysal V and Perc M 2016 *Sci. Rep.* **6** 30914
[13] Zhao Z and Gu H 2017 *Sci. Rep.* **7** 6760
[14] Strukov D B, Snider G S, Stewart D R, Williams and Stanley R 2008 *Nature* **453** 80
[15] Chua L O 2015 *Radioengineering* **24** 319
[16] Wang C, Xiong L, Sun J and Yao W 2019 *Nonlinear Dyn.* **95** 2893
[17] Mannan Z I, Adhikari S P, Yang C, Budhathoki R K, Kim H and Chua L 2019 *IEEE Trans. Neural Netw. Learn. Syst.* **30** 3458
[18] Wang C, Guo S and Xu Y 2017 *Complexity* **2017** 5436737
[19] Wang H, Ma J and Chen Y 2014 *Commun. Nonlinear Sci. Numer. Simulat.* **19** 3242
[20] Ma J, Song X, Jin W and Wang C 2015 *Chaos Solitons Fract.* **80** 31
[21] Qu L, Du L, Zhang H and Cao Z 2019 *Int. J. Bifurcat. Chaos* **29** 1950202
[22] Yilmaz E, Baysal V, Perc M and Ozer M 2016 *Sci. China Technol. Sc.* **59** 364
[23] Tripathi D, Pandey S K and Das S 2015 *Appl. Math. Comput.* **215** 3645
[24] Hilfer R 2000 *Applications of Fractional Calculus in Physics*, 2nd edn. (Singapore: World Scientific) pp. 12–15
[25] Monje C A, Chen Y Q, Vinagre B M and Xue D 2010 *Fractional-order Systems and Controls*, 1st edn. (Springer Science & Business Media) pp. 89–162
[26] Lundstrom B N, Higgs M H, Spain W J and Fairhall A L 2018 *Nat. Neurosci.* **11** 1335
[27] Magin R L 2014 *Critical Review in Biomedical Engineering* **32** 10
[28] Yu Y, Shi M, Kang H, Chen M and Bao B 2020 *Nonlinear Dyn.* **100** 891
[29] Alidousti J and Ghaziani 2017 *Mathematical Models and Computer Simulations* **9** 390
[30] Meng F, Zeng X and Wang Z 2019 *Nonlinear Dyn.* **95** 1615
[31] Meng F, Zeng X and Wang Z 2020 *Int. J. Bifurcat. Chaos* **30** 2050044
[32] Malik S A and Mir A H 2020 *IEEE ACM T. Comput. Bi.* **11** 1545
[33] Leng Y, Yu D, Hu Y, Yu S and Ye Z 2020 *Chaos* **30** 033108
[34] Chua L O 2005 *Int. J. Bifurcat. Chaos* **15** 3435

[35] Chua L O 2014 *Semicond. Sci. Tech.* **29** 104001
[36] Gibson GA, Musunuru S, Zhang J, Vandenberghe K, Lee J and Cheng C 2016 *Appl. Phys. Lett.* **108** 023505
[37] Li Z, Guo Z, Wang M and Ma M 2021 *AEU-Int. J. Electron. Commun.* **142** 153995
[38] Jin P, Wang G, Lu H and Fernando T A 2017 *IEEE T. Circuits Sys. II* **65** 246
[39] Xu B, Wang G, Lu H, Yu S and Yuan F 2019 *Nonlinear Dyn.* **96** 765
[40] Yuan F, Wang G and Wang X 2016 *Chaos* **26** 073107
[41] Zhu M, Wang C, Deng Q and Hong Q 2020 *Int. J. Bifurcat. Chaos* **30** 2050184
[42] Li Z, Zhou H, Wang M and Ma M 2021 *Nonlinear Dyn.* **104** 1455
[43] Lin H, Wang C, Sun Y and Wei Y 2020 *Nonlinear Dyn.* **100** 3667
[44] Li Z and Zhou H 2021 *Electron. Lett.* **57** 715
[45] Xie W, Wang C and Lin H 2021 *Nonlinear Dyn.* **104** 4523
[46] Yang N, Xu C, Wu C, Jia R and Liu C 2019 *Nonlinear Dyn.* **97** 33
[47] Chang H, Wang Z, Li Y and Chen G 2018 *Int. J. Bifurcat. Chaos* **28** 1850105
[48] Matignon D 2016 *Computational Engineering in Systems Applications* **2** 963
[49] Adomian G 1998 *J. Math. Anal. Appl.* **135** 501
[50] Tavazoei M S and Haeri M 2009 *Automatica* **45** 1886
[51] Kaslik E and Sivasundaram S 2012 *Nonlinear Anal.* **13** 1489
[52] Danca M F, Fečkan M, Kuznetsov N V and Chen G 2018 *Nonlinear Dyn.* **91** 2523
[53] Danca M F, Fečkan M and Chen G 2017 *Nonlinear Dyn.* **89** 1889
[54] Kang Y M, Xie Y, Lu J C and Jiang J 2015 *Nonlinear Dyn.* **82** 1259
[55] Izhikevich E M 2000 *Int. J. Bifurcat. Chaos* **10** 1171
[56] Danca M F and Kuznetsov N 2018 *Int. J. Bifurcat. Chaos* **28** 1850067
[57] Bandy D K, Burton E K, Hall J R, Chapman D M and Elrod J T 2021 *Chaos* **31** 013120
[58] Hall J R, Burton E K, Chapman D M and Bandy D K 2021 *Applied Sciences* **11** 9905
[59] Chen X, Liu C and Wang F 2008 *Chin. Phys. B* **17** 1664
[60] Shao S, Min F and Ma M 2013 *J. Phys.* **62** 130504 (in Chinese)
[61] Zhou C, Li Z and Xie F 2019 *Eur. Phys. J. Plus* **134** 73